

ELEMENTARY PARTICLES AND FIELDS
Experiment

**Detection of Charged Charmed D^\pm Mesons in Proton–Nucleus
Interaction at 70 GeV with the SVD-2 Setup**

V. N. Ryadovikov*
(On behalf of the SVD-2 Collaboration¹⁾)

Institute for High Energy Physics, pl. Nauki 1, Protvino, Moscow oblast, 142281 Russia

Received November 6, 2013

Abstract—The results of processing data stemming from the SERP-E-184 experiment devoted to studying the mechanisms of the production of charmed particles in proton–nucleus interactions at 70 GeV and the decays of these particles with the aid of the SVD-2 setup are presented. Those data were obtained upon irradiating, with a 70-GeV proton beam, the SVD-2 active target consisting of carbon, silicon, and lead plates. A detailed simulation based on the FRITIOF7.02 and GEANT3.21 packages made it possible to optimize event-selection criteria and to calculate the detection efficiencies for D^\pm mesons. After the separation of a signal from the three-body decay of charged charmed D^\pm mesons, the inclusive cross sections for their production at threshold energies were measured along with respective lifetimes and parameters of the A dependence of the cross sections. The yields of D mesons and their ratios are compiled in a table along with data from other experiments and the respective theoretical predictions.

DOI: 10.1134/S106377881406012X

INTRODUCTION

Studies devoted to exploring features of the production neutral charmed mesons in proton–nucleus interaction at 70 GeV by using the SVD-2 setup (SERP-E-184 experiment [1]) permitted estimating the charm-production cross section $\sigma(c\bar{c})$ at the threshold energy [2–4]. It was shown that the experimental situation prevalent in that energy region is contradictory and that theoretical estimates of respective cross sections are highly sensitive to parameters of QCD models. In view of this, further measurements of the yields of various charmed particles are of great topical interest. In this article, we present the results obtained by analyzing data that arise upon the selection of events involving the decays

$D^+ \rightarrow K^- \pi^+ \pi^+$ and $D^- \rightarrow K^+ \pi^- \pi^-$ in proton–nucleus interaction at 70 GeV. The cross sections for the production of charged charmed mesons and their yields were estimated, and some properties of D^\pm mesons are studied.

PRELIMINARY EVENT-SELECTION
CRITERIA

In our analysis, we employed 52 million inelastic events detected by using three nuclear targets manufactured from carbon, silicon, and lead. For a detailed description of the SVD-2 setup used in our experiment devoted to studying the production of charmed particles in proton–nucleus interaction at 70 GeV, the interested reader is referred to [5]. Because of a moderately small cross section for the production of charmed particles at threshold energies, their short path length, and the deteriorating reconstruction efficiency for all tracks at the multi-particle decay vertex, stringent criteria were not used in the primary selection of events possibly featuring the production of charmed particles. The required class of events was selected by applying the followed procedures: (i) reconstruction of tracks and the primary vertex in projections according to data from a vertex detector (VD); (ii) searches for secondary two-prong vertices (vees) in the track-parameter space $\{a, b\}$ [2], this procedure being a fast filter for the selection of events possibly involving the production

*E-mail: riadovikov@ihep.ru

¹⁾ A. N. Alev, E. N. Ardashev, A. G. Afonin, V. P. Balandin, S. G. Basiladze, S. F. Berezhnev, G. A. Bogdanova, M. Yu. Bogolyubsky, A. M. Vischnevskaya, V. Yu. Volkov, A. P. Vorobiev, A. G. Voronin, V. F. Golovkin, S. N. Golovnia, S. A. Gorokhov, N. I. Grishin, Ya. V. Grishkevich, G. G. Ermakov, P. F. Ermolov, V. N. Zapolsky, E. G. Zverev, D. E. Karmanov, V. I. Kireev, A. A. Kiriakov, V. N. Kramarenko, A. V. Kubarovsky, N. A. Kouzmine, L. L. Kurchaninov, G. I. Lanshikov, A. K. Leflat, S. I. Lyutov, M. M. Merkin, G. Ya. Mitrofanov, V. S. Petrov, Yu. P. Petukhov, A. V. Pleskach, V. V. Popov, V. M. Ronjin, V. A. Senko, M. M. Soldatov, L. A. Tikhonova, N. F. Furmanec, A. G. Kholodenko, Yu. P. Tsyupa, N. A. Shalanda, A. I. Yukaev, V. I. Yakimchuk.

of charmed particles; (iii) spatial reconstruction of tracks of charged particles in a magnetic spectrometer (MS) and a determination of their momenta; (iv) searches for secondary three-prong vertices with the aid of a further analysis of tracks in the $\{a, b\}$ space with allowance for their charge and for kinematical correspondence to the primary interaction vertex; and (v) a determination of the decay-particle momentum with the aid of the condition $P > 7$ GeV (see below).

After implementing the aforementioned procedures, 16320 events compatible with $D^+ \rightarrow K^- \pi^+ \pi^+$ decay hypothesis and 8439 events compatible with the $D^- \rightarrow K^+ \pi^- \pi^-$ decay hypothesis remain for a further analysis. The experimental effective-mass spectra of the $K^- \pi^+ \pi^+$ and $K^+ \pi^- \pi^-$ systems for these events are shown in Fig. 1 along with their approximations obtained by fitting to them a superposition of a Gaussian function and a polynomial of sixth degree. One can see signals in the D -meson region, but they have a substantial background pedestal.

SIMULATION AND OPTIMIZATION OF CRITERIA FOR SELECTING EVENTS INVOLVING THE PRODUCTION OF CHARMED PARTICLES

The GEANT3.21 code package [6] supplemented with a geometric description of all elements of the SVD-2 setup was used to simulate events and to optimize criteria for selecting events that involve the production of charmed particles in the experiment being discussed. Proton–nucleus interactions were generated by means of the FRITIOF7.02 code [7]. By employing the GEANT code, ten million events obtained by a Monte Carlo method where the production of charmed particles was forbidden were passed through the data-processing system in order to simulate background conditions. Because of the simulation of noise effects in the experiment and because of the imperfection of the algorithm for reconstructing events involving three-body decays, spurious three-prong decay vertices (background) were found in some events. In those events, the distributions with respect to the parameters of the $K^- \pi^+ \pi^+$ system were compared with the experimental background. As the experimental background, we selected events in which the effective mass of the $K^- \pi^+ \pi^+$ system fell within the interval obtained from the distribution in Fig. 1—that is, in the interval of $M = 1.858 \pm (3 \cdot 0.018)$ GeV. The same requirements were applied to Monte Carlo events. Figure 2 shows the distributions of the reduced path length ($L_{\text{path}} = L \times M/P$), momentum (P), and Feynman variable ($x_F = 2P_{\parallel}^*/\sqrt{s}$ in the c.m. frame) of the $K^- \pi^+ \pi^+$ system. All of the distributions were normalized to unity in area. One

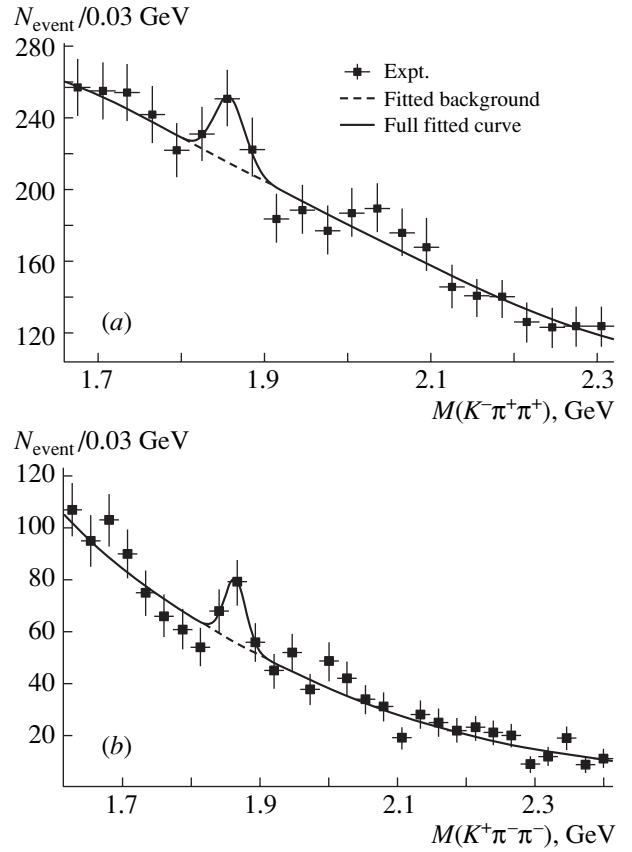


Fig. 1. Effective-mass spectra of the (a) $K^- \pi^+ \pi^+$ and (b) $K^+ \pi^- \pi^-$ systems after the primary selection of events featuring three-prong vertices.

can see that there is good agreement between Monte Carlo events and experimental data. Thus, simulated events faithfully reproduce background conditions of the experiment.

In order to optimize the set of criteria for selecting events involving the production of charmed particles, two samples each containing 500 thousand Monte Carlo events involving the decay $D^+ \rightarrow K^- \pi^+ \pi^+$ (in one) and $D^- \rightarrow K^+ \pi^- \pi^-$ (in the other) were generated with the aid of the GEANT code. A simulation reveals that, because of the acceptance of the setup, the reconstruction of all tracks in the decay vertex is possible provided that the decay-particle momentum is in excess of 7 GeV. At the first stage, we analyzed the Dalitz plot for the decay $D^+ \rightarrow K^- \pi^+ \pi^+$, determining the phase-space boundaries characteristic of the three-body decay being considered. We analyzed the two-dimensional histogram of mass hypotheses for the systems in question: $m_1(K^- \pi_1^+)$ and $m_2(K^- \pi_2^+)$. From the kinematics of three-body decay, it follows that, for the Dalitz plot, the boundary conditions have the form

$$m_{1\text{max}} = m_{2\text{max}} = m_D - m_\pi \approx 1.73 \text{ GeV}, \quad (1)$$

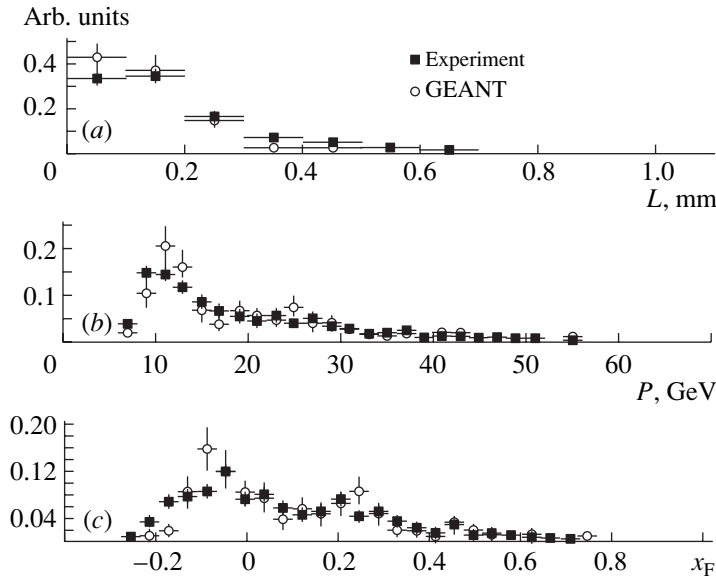


Fig. 2. Distributions with respect to the following parameters of the $K^- \pi^+ \pi^+$ system for background events: (a) reduced path length (see main body of the text), (b) momentum, and (c) Feynman variable.

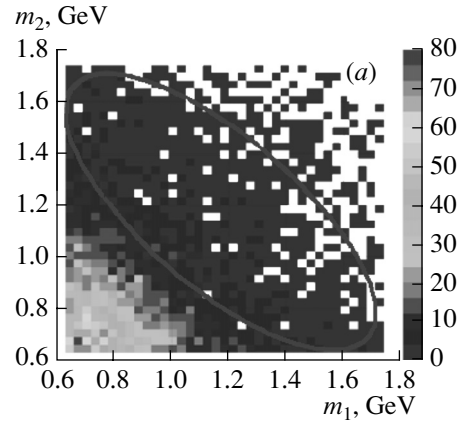
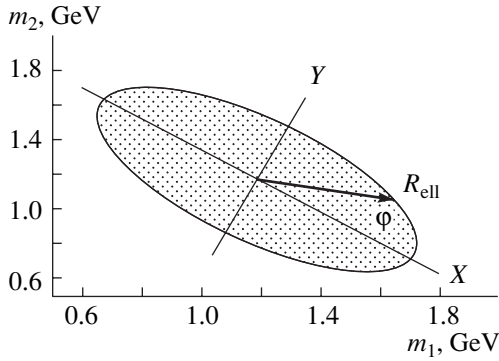


Fig. 3. Dalitz plot for the $K^- \pi^+ \pi^+$ system in Monte Carlo events.

$$m_{1 \min} = m_{2 \min} = m_K + m_\pi \approx 0.63 \text{ GeV.}$$

Figure 3 presents an approximation of the phase space by an ellipse for Monte Carlo–simulated events; that is,

$$\begin{aligned} X &= (m_1 - \Delta m_1) \cos \theta + (m_2 - \Delta m_2) \sin \theta, \quad (2) \\ Y &= (m_2 - \Delta m_2) \cos \theta - (m_1 - \Delta m_1) \sin \theta, \\ X^2/R_X^2 + Y^2/R_Y^2 &= 1, \end{aligned}$$

where $\Delta m_1 = 1.18 \text{ GeV}$, $\Delta m_2 = 1.17 \text{ GeV}$, and $\theta = 44.78^\circ$ are parameters that accomplish a transition to the coordinate frame associated with the ellipse (X, Y) and R_X and R_Y are the semiaxes of the ellipse.

Figure 4a shows the Dalitz plot of the $K^- \pi^+ \pi^+$ system for experimental events upon the superimposition of the ellipse in question and with allowance for the boundary conditions in (1), while Fig. 4b

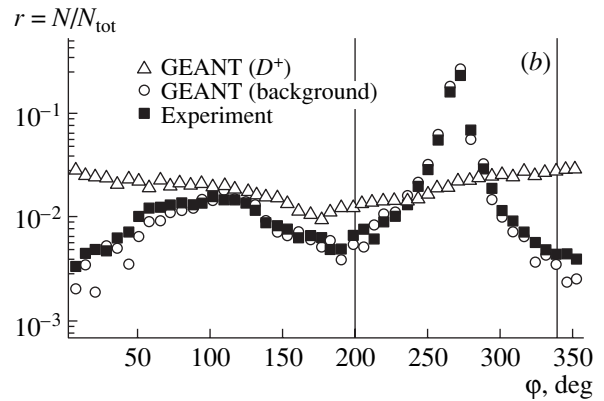


Fig. 4. (a) Calculated kinematical ellipse on the experimental Dalitz plot for the $K^- \pi^+ \pi^+$ system; (b) density of experimental and Monte Carlo events versus the angle φ .

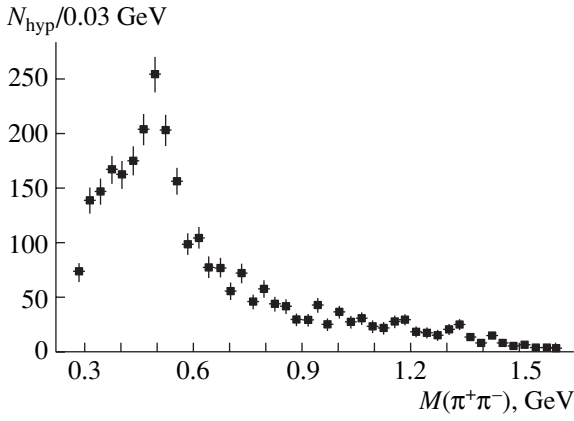


Fig. 5. Effective-mass spectrum of the $\pi^+\pi^-$ system for two K^0 hypotheses from the experimental sample of three-body vertices after the application of selection criteria.

gives the density distributions of experimental and Monte Carlo–simulated events in the ellipse coordinate frame (see Fig. 3). From the distribution with respect to the angle φ , it can be seen that a dominant part of the background under the D^+ signal (Fig. 1a) is concentrated in the angular range of $270^\circ \pm 70^\circ$. In order to reduce the background pedestal, we selected events from the regions of $\varphi < 200^\circ$, $\varphi > 340^\circ$, and $R_{\text{ell}} < 1$. In the region of φ between 30° and 170° , the density of Monte Carlo–simulated events involving D^+ decays is commensurate with the density of background events; therefore, we did not exclude this region from a further analysis.

A significant part of the background is formed upon the superimposition of the charged-particle track issuing from the interaction vertex on the K^0 -meson-decay vertex. If, in the $K^-\pi^+\pi^+$ system, one replaces the K^- hypothesis for the negative track by the π^- hypothesis, there arises two hypotheses for K^0 -meson decay. The effective-mass spectrum of the $\pi^+\pi^-$ system for two K^0 hypotheses from the experimental sample of three-body vertices is presented in Fig. 5 with allowance for the selection criteria presented above. In order to exclude this background, we consider the two-dimensional histogram in Fig. 6a. From this figure, it can be seen that the contribution from the K^0 background is concentrated in the lower part of the diagram bounded by a line; that is,

$$M(\pi^+\pi^-)_{\text{H1}} + M(\pi^+\pi^-)_{\text{H2}} < C. \quad (3)$$

The ratio of the number of events under the straight line specified by Eq. (3) to the total number of events ($W = N_{\text{cut}}/N_{\text{tot}}$) depends on the parameter C . The value of $C = 1.2$ was obtained from an analysis of the dependences $W(C)$ for experimental and Monte

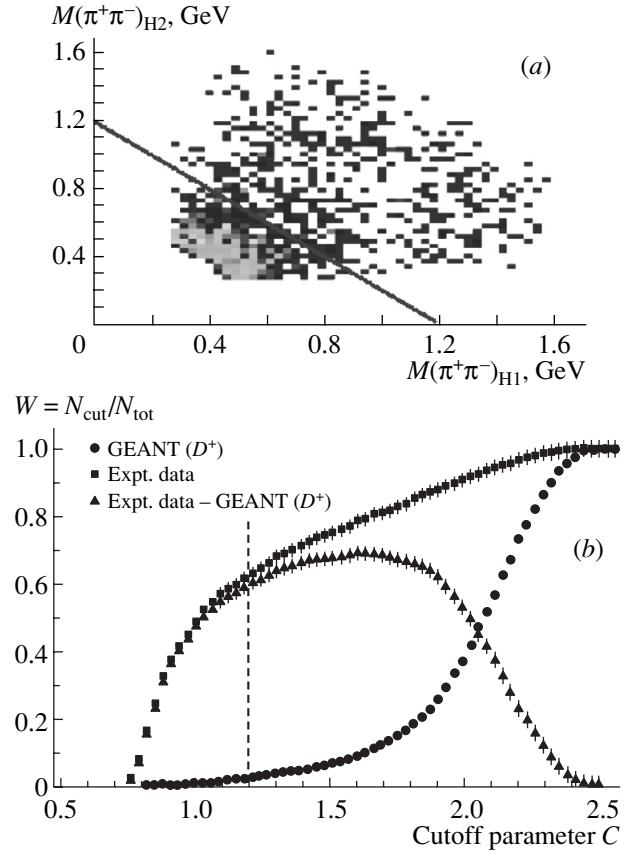


Fig. 6. (a) Two-dimensional histogram for the $\pi^+\pi^-$ system (the line represents the boundary for excluding the K^0 -meson background); (b) W (see main body of the text) as a function of the cutoff parameter C .

Carlo–simulated events in Fig. 6b. Figure 7 gives the effective-mass spectrum of the $\pi^+\pi^-$ system for two K^0 hypotheses from the experimental sample for D^+ after the exclusion of the region shown in Fig. 6.

Figure 8 shows the distributions with respect to the reduced path length L_{path} of the $K^-\pi^+\pi^+$ system for Monte Carlo–simulated events involving D^+ decay and a background secondary three-prong vertex. On the basis of an analysis of the distributions in Fig. 8, we introduced the condition $L_{\text{path}} > 0.12$ mm.

A similar analysis of selection criteria was performed for events possibly featuring the decay $D^- \rightarrow K^+\pi^-\pi^-$.

ANALYSIS OF EXPERIMENTAL EVENTS AFTER THE APPLICATION OF SELECTION CRITERIA

After performing the simulation in question, we have chosen event-selection criteria that ensure a

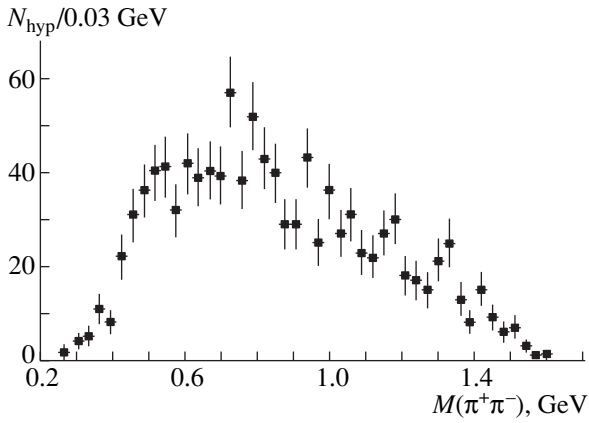


Fig. 7. Effective-mass spectrum of the $\pi^+\pi^-$ system for two K^0 hypotheses from the experimental sample for D^+ after the elimination of the region shown in Fig. 6.

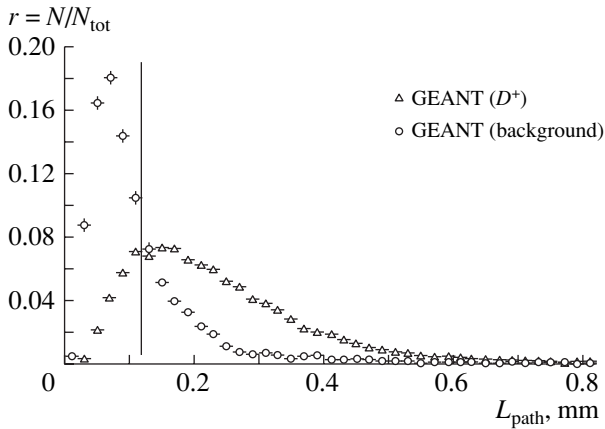


Fig. 8. Distribution with respect to the reduced path length of the $K^-\pi^+\pi^+$ system for Monte Carlo-simulated events. The line represents the boundary of event selection.

minimum background. For the decay process $D^+ \rightarrow K^-\pi^+\pi^+$, these criteria are the following:

$$\varphi(K^-\pi^+) < 200^\circ, \quad \varphi(K^-\pi^+) > 340^\circ$$

$$\text{и } R_{\text{ell}} < 1 \text{ (Fig. 4);}$$

$$M(\pi^+\pi^-)_{\text{H1}} + M(\pi^+\pi^-)_{\text{H2}} > 1.2 \text{ GeV (Fig. 6);}$$

$$L_{\text{np}}(K^-\pi^+\pi^+) > 0.12 \text{ mm (Fig. 8).}$$

Figure 9 shows the effective-mass spectrum of the $K^-\pi^+\pi^+$ system for experimental events after the application of all selection criteria. After parametrizing the spectrum in Fig. 9 in terms of a superposition of a Gaussian function and a polynomial of fifth degree ($\chi^2/\text{NDF} = 13.5/30$), we obtain 15.5 signal events from D^+ -meson decay and 16.6 events in the background pedestal. The measured D^+ -meson mass is 1874 ± 5 MeV (the world-average value is

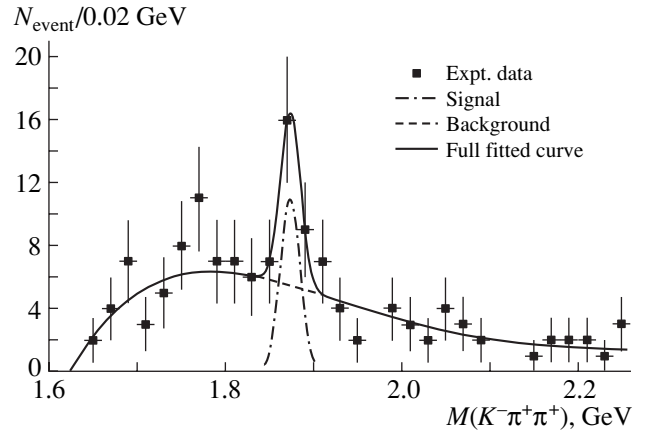


Fig. 9. Effective-mass spectrum of the $K^-\pi^+\pi^+$ system for experimental events after the application of all selection criteria.

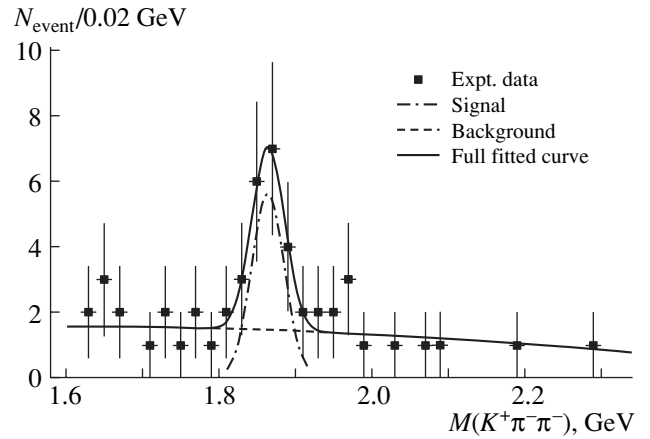


Fig. 10. Effective-mass spectrum of the $K^+\pi^-\pi^-$ system for experimental events after the application of all selection criteria.

1869.6 MeV), the root-mean-square deviation being 11.5 MeV. In the region around the D^+ -meson mass, there is no background from the K^0 -meson admixture. The selection efficiency obtained for a signal of D^+ -meson decay from the simulation and determined as the ratio of the number of events in the signal after all cuts to the total number of Monte Carlo-simulated events involving the decay $D^+ \rightarrow K^-\pi^+\pi^+$ is $\varepsilon(D^+) = 0.014$. The condition requiring that identical procedures be applied to processing experimental and simulated events was respected here.

Similar procedures were implemented for selecting of D^- -meson signal (Fig. 10) in the mass spectrum of the $K^+\pi^-\pi^-$ with the same event-selection criteria. The effective-mass spectrum of the $K^+\pi^-\pi^-$ system in Fig. 10 was also parametrized in terms of a superposition of a Gaussian function and a polynomial of

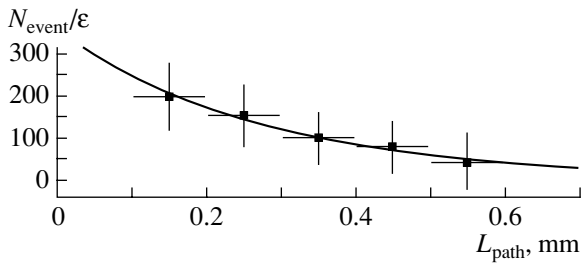


Fig. 11. Reconstructed experimental path length of a D^+ meson with allowance for the detection efficiency.

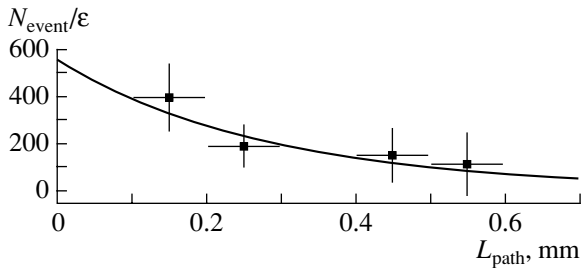


Fig. 12. As in Fig. 11, but for a D^- meson.

second degree ($\chi^2/\text{NDF} = 3.6/20$). The number of signal events was 15.0, while the background under the signal was 8.7 events. The D^- -meson mass is 1864 ± 8 MeV, while the the root-mean-square deviation is 22 MeV. The selection efficiency obtained from the simulation for the D^- -meson signal is $\varepsilon(D^-) = 0.008$.

LIFETIME OF D^\pm MESONS

In the effective-mass spectrum of the $K^-\pi^+\pi^+$ system (Fig. 9), we singled out the signal band of $M(D^+) \pm 2.5\sigma$ according to fitted parameters and constructed the distribution of the reduced path length L_{path} for these events. The inclusion of the background pedestal was performed on the basis of the L_{path} distribution for background events off the

signal interval in the mass spectrum. After that, the experimental distribution of L_{path} was reconstructed with allowance for the detection efficiency (ε) obtained from the simulation for D^+ events in the L_{path} interval being considered (Fig. 11) and was approximated by the function $\exp(-L/c\tau)$. By using the fitted value of the exponent, we have estimated the parameter $c\tau$ at $c\tau = 291 \pm 75 \mu\text{m}$ [the world-average value of this parameter is $c\tau(D^+) = 311.8 \mu\text{m}$]. By similarly measuring the D^- -meson lifetime (Fig. 12), we obtained $c\tau = 341 \pm 88 \mu\text{m}$. The errors in the parameter $c\tau$ are purely statistical. The proximity of the measured D^\pm -meson lifetimes to the world-average value confirm the detection of charmed particles in our experiment. The estimates of $c\tau$ for regions off the signal region differ substantially from those values.

CROSS SECTIONS FOR D^\pm -MESON PRODUCTION AND THEIR MASS-NUMBER DEPENDENCE

In order to calculate cross sections for D -meson production on target nuclei, we used the expression

$$N_s = [N_0 \times (\sigma_D \times A^\alpha) / (\sigma_{pp} \times A^{0.7})] \times [(B \times \varepsilon) / K_{\text{tr}}],$$

where N_s is the number of signal events that was obtained from an analysis of mass spectra for each target-nucleus sort (see Table 1); N_0 is the number of events involving proton–nucleus interactions in the target (see Table 1); σ_D is the cross section for charmed-particle production; A is the atomic weight of the target material (C, Si, or Pb); α is the exponent in the A dependence of the cross section for the production of charmed particles (in the cross section for inelastic proton–nucleus interactions, this exponent is taken to be 0.7); σ_{pp} is the cross section for inelastic proton–proton interaction at the energy of 70 GeV ($31\,440 \mu\text{b}$); B is the branching ratio for the decay $D^\pm \rightarrow K\pi\pi$ (0.094); ε is the detection efficiency for D mesons: $\varepsilon(D^+) = 0.014$ and $\varepsilon(D^-) = 0.008$; and $K_{\text{tr}} = 0.57$ (refined triggering coefficient—that is, the degree of suppression of the detection of inelastic events in the course of data accumulation [3]).

Upon making the substitution $C_D = [N_0 / (\sigma_{pp} \times A^{0.7})] \times [(B \times \varepsilon) / K_{\text{tr}}]$, we obtain

$$N_s = C_D \times \sigma_D \times A^\alpha$$

or

$$\ln(N_s/C_D) = \alpha \times \ln(A) + \ln(\sigma_D).$$

Figure 13 shows the cross section for the production of charmed particles in a target material as a function of A . After approximating this dependence by a straight line, we estimate the parameter α in the

Table 1. Parameter values for calculating cross sections

Parameter	C	Si	Pb
A	12	28	207
N_0	11.37×10^6	27.44×10^6	13.19×10^6
D^+			
N_s	2	8	6
D^-			
N_s	2	7	6

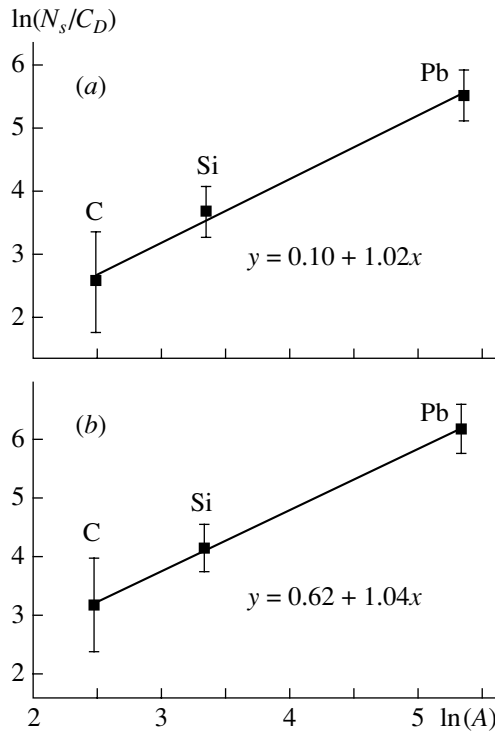


Fig. 13. Cross sections for (a) D^+ and (b) D^- production in a target material (C, Si, or Pb) versus A .

A dependence at $\alpha = 1.02 \pm 0.26$ for events involving D^+ production and at $\alpha = 1.04 \pm 0.27$ for events involving D^- production. The errors in the values of the parameter α are purely statistical.

The resulting parametrization of the A dependence leads to the following target-nucleus-weighted mean values of the total inclusive cross sections:

$$\sigma(D^+) = 1.2 \pm 0.4(\text{stat.}) \pm 0.2(\text{syst.}) \mu\text{b/nucleon},$$

$$\sigma(D^-) = 1.9 \pm 0.6(\text{stat.}) \pm 0.4(\text{syst.}) \mu\text{b/nucleon}.$$

The relative errors in these cross sections stem from the statistics of signals (about 30%) and from uncertainties in calculating the efficiencies and triggering coefficient (about 15%).

RATIOS OF CHARMED-PARTICLE YIELDS

On the basis of the results obtained by detecting neutral D mesons, the total cross section for the production of charmed particles in proton–nucleus interaction at 70 GeV was estimated earlier in [3] at

$$\sigma(c\bar{c}) = 7.1 \pm 2.4(\text{stat.}) \pm 1.4(\text{syst.}) \mu\text{b/nucleon}.$$

On the basis of these data, the yield of charged charmed D mesons was estimated at 17% for D^+ mesons and at 27% for D^- mesons.

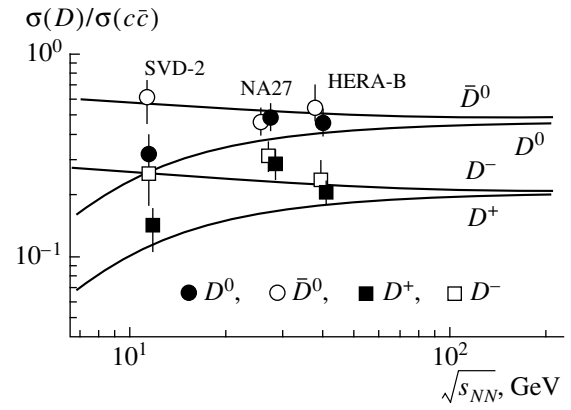


Fig. 14. Relative yields of charmed mesons. The displayed experimental points were taken from Table 2, while the theoretical curves were borrowed from [8].

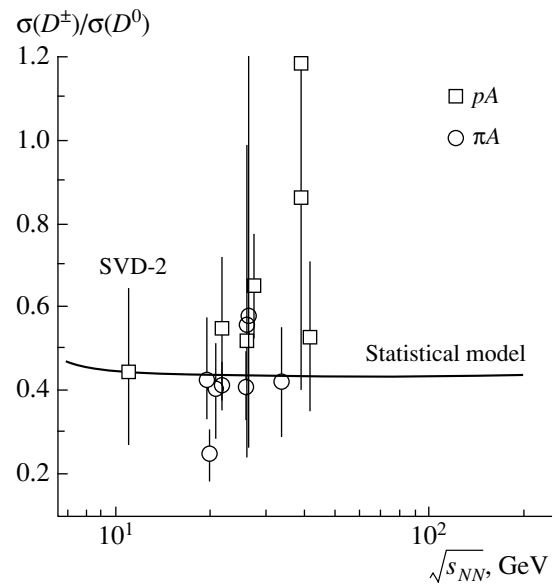


Fig. 15. Ratios of the cross sections for the production of charged and neutral D mesons.

On the basis of the results reported in [3], the total inclusive cross sections for the production of neutral charmed mesons were estimated at

$$\sigma(D^0) = 2.5 \pm 0.8(\text{stat.}) \pm 0.5(\text{syst.}) \mu\text{b/nucleons},$$

$$\sigma(\bar{D}^0) = 4.6 \pm 1.6(\text{stat.}) \pm 0.9(\text{syst.}) \mu\text{b/nucleon}.$$

The ratio of the yields of charged and neutral D mesons is $(D^+ + D^-)/(D^0 + \bar{D}^0) = 44\%$. The D -meson yields measured in that experiment and their ratios are given in Table 2 and in Fig. 14 along with data from other two known experiments and with theoretical predictions for a 70-GeV proton beam. The particle yields and their ratios were either taken from [9, 10] or calculated on the basis of data presented in those articles.

Table 2. Ratios of charmed-particle yields

Yields and ratio of yields of D mesons	PYTHIA pp	FRITIOF			SVD-2 pA	Other experiments	
		C	Si	Pb		NA-27	HERA-B
D^0	0.28	0.48	0.51	0.55	0.35 ± 0.16	0.57 ± 0.08	0.44 ± 0.18
\bar{D}^0	0.74	0.60	0.59	0.58	0.65 ± 0.31	0.43 ± 0.09	0.54 ± 0.23
D^+	0.13	0.28	0.29	0.29	0.16 ± 0.07	0.31 ± 0.06	0.19 ± 0.08
D^-	0.24	0.28	0.27	0.28	0.27 ± 0.17	0.34 ± 0.06	0.25 ± 0.11
D^0/\bar{D}^0	0.38	0.80	0.86	0.95	0.54 ± 0.25	1.33 ± 0.25	0.81 ± 0.23
D^+/D^-	0.54	1.0	1.1	1.0	0.59 ± 0.20	0.92 ± 0.21	0.76 ± 0.22
$D^\pm/(D^0 + \bar{D}^0)$	0.36	0.51	0.51	0.5	0.44 ± 0.24	0.65 ± 0.21	0.46 ± 0.18
D^+/D^0	0.18	0.56	0.56	0.52	0.46 ± 0.21	0.54 ± 0.11	0.44 ± 0.12
D^-/\bar{D}^0	0.32	0.47	0.46	0.48	0.42 ± 0.26	0.78 ± 0.19	0.47 ± 0.14

From Table 2 and from Fig. 14, one can see that the contributions of charged and neutral D mesons to the total cross sections for open-charm production in proton–nucleus interactions change with interaction energy. For example, the D^0 - and D^+ -meson contributions show a trend toward reduction as the interaction energy decreases to 70 GeV, while the \bar{D}^0 - and D^- -meson contributions grow; that is, the difference of the particle and antiparticle contribution to the cross sections for open-charm production in proton–nucleus interaction grows as the interaction energy decreases.

A large difference of the charmed-particle and charmed-antiparticle yields was first observed experimentally in neutron–nucleus interaction at an intermediate neutron-beam energy of 43 GeV in the BIS-2 experiment, where antiparticle (\bar{D}^0 - and D^- -meson) decays were observed [11], while particle (D^0 - and D^+ -meson) decays were not found. The particle-production cross sections proved to be below the sensitivity threshold in that experiment. This behavior of the D -meson contributions to the charm-production cross section can be explained by the possible nuclear-matter effect on the production of respective particles. The mechanisms behind this effect were considered in a number of theoretical studies [12]. The results that we obtained for the D -meson yields (Fig. 14) are compared with the predictions of the statistical-hadronization model [8, 13].

The cross sections for the production of charged and neutral D mesons from [14] are shown in Fig. 15 along with the result obtained in the present study. The data are also compared with the results of the calculations based on the statistical model [13].

CONCLUSIONS

In the SERP-E-184 experiment aimed at searches for the production of charmed particles and at studying their properties in proton–nucleus interactions at 70 GeV with the aid of SVD-2 setup, we have singled out signals from the decays of charged D^\pm mesons in the effective-mass spectra of $(K\pi\pi)$ three-body systems. On the basis of a detailed simulation with the aid of the FRITIOF7.02 and GEANT3.21 codes, we have optimized event-selection criteria and calculated detection efficiencies for D^\pm mesons. The resulting inclusive cross sections for D^\pm -meson production at the threshold energies are

$$\begin{aligned}\sigma(D^+) &= 1.2 \pm 0.4(\text{stat.}) \pm 0.2(\text{syst.}) \mu\text{b/nucleon}, \\ \sigma(D^-) &= 1.9 \pm 0.6(\text{stat.}) \pm 0.4(\text{syst.}) \mu\text{b/nucleon}.\end{aligned}$$

The presence of plates from various materials (C, Si, and Pb) in the active target of the SVD-2 setup has made it possible to measure parameters in the A dependence of the cross sections for D^\pm -meson production. The results are

$$\begin{aligned}\alpha &= 1.02 \pm 0.26 \text{ for } D^+, \\ \alpha &= 1.04 \pm 0.27 \text{ for } D^-.\end{aligned}$$

By using the results obtained previously by estimating the total cross section for the production of charmed particles [3] and the cross sections for the production of neutral D^0 (\bar{D}^0) mesons, we have determined the yields of D^\pm mesons and their ratios and compared them with data from other experiments and with theoretical predictions. The experimental data on the yields of charmed particles in the threshold region of energies of proton–nucleus interactions are close to the respective predictions

REFERENCES

1. E. N. Ardashev et al., Preprint No. 96-98, IFVE (Inst. High Energy Phys., Protvino, 1996); <http://web.ihep.su/library/pubs/ps/96-98.pdf>.
2. A. P. Vorob'ev et al., Preprint No. 2008-17, IFVE (Inst. High Energy Phys., Protvino, 2008); <http://web.ihep.su/library/pubs/ps/2008-17.pdf>.
3. V. N. Ryadovikov (on behalf of SVD-2 Collab.), Phys. At. Nucl. **73**, 1539 (2010); <http://web.ihep.su/library/pubs/ps/2009-09.pdf>. <http://arxiv.org/abs/1004.3676>.
4. V. N. Ryadovikov (on behalf of SVD-2 Collab.), Phys. At. Nucl. **74**, 324 (2011); <http://web.ihep.su/library/pubs/ps/2010-2.pdf>. [arXiv:1106.1563](http://arxiv.org/abs/1106.1563).
5. V. V. Avdeichikov et al., Instrum. Exp. Tech. **56**, 9 (2013).
6. GEANT3.21, CERN Program Library Long Writeup W5013.
7. H. Pi, Comput. Phys. Commun. **71**, 173 (1992).
8. A. Andronic *et al.*, Phys. Lett. B **659**, 149 (2008); [arXiv:0708.1488v1](http://arxiv.org/abs/0708.1488v1).
9. LEBC-EHS Collab., Phys. Lett. B **189**, 476 (1987).
10. I. Abt et al., Eur. Phys. J. C **52**, 531 (2007); [arXiv:0708.1443v1](http://arxiv.org/abs/0708.1443v1).
11. A. Aleev et al., Z. Phys. C **37**, 243 (1988).
12. L. Tolos, J. Schaffner-Bielich, and H. Stöcker, Phys. Lett. B **635**, 85 (2006); [nucl-th/0509054](http://arxiv.org/abs/nucl-th/0509054); K. Tsushima, D. H. Lu, A. W. Thomas, et al., Phys. Rev. C **59**, 2824 (1999); [nucl-th/9810016](http://arxiv.org/abs/nucl-th/9810016); A. Sibirtsev, K. Tsushima, and A. W. Thomas, Eur. Phys. J. A **6**, 351 (1999); [nucl-th/9904016](http://arxiv.org/abs/nucl-th/9904016); A. Sibirtsev, K. Tsushima, K. Saito, and A. W. Thomas, Phys. Lett. B **484**, 23 (2000); [nucl-th/9904015](http://arxiv.org/abs/nucl-th/9904015); A. Hayashigaki, Phys. Lett. B **487**, 96 (2000); [nucl-th/0001051](http://arxiv.org/abs/nucl-th/0001051); W. Cassing, E. L. Bratkovskaya, and A. Sibirtsev, Nucl. Phys. A **691**, 753 (2001); [nucl-th/0010071](http://arxiv.org/abs/nucl-th/0010071); B. Friman, S. H. Lee, and T. Song, Phys. Lett. B **548**, 153 (2002); [nucl-th/0207006](http://arxiv.org/abs/nucl-th/0207006); M. F. M. Lutz and C. L. Korpa, Phys. Lett. B **633**, 43 (2006); [nucl-th/0510006](http://arxiv.org/abs/nucl-th/0510006); K. Morita and S. H. Lee, [arXiv:0704.2021](http://arxiv.org/abs/0704.2021).
13. A. Andronic, F. Beutler, P. Braun-Munzinger, et al., [arXiv:0904.1368v2](http://arxiv.org/abs/0904.1368v2).
14. C. Lourenco and N. K. Wöhri, Phys. Rep. **433**, 127 (2006); [hep-ph/0609101](http://arxiv.org/abs/hep-ph/0609101).